Journal of Cardiovascular Magnetic Resonance®, 3(4), 339–347 (2001)

Myocardial Fiber Orientation Mapping Using Reduced Encoding Diffusion Tensor Imaging

Edward W. Hsu[1,2] and Craig S. Henriquez[1]

[1]*Department of Biomedical Engineering, Duke University, Durham, North Carolina*
[2]*Center for* In Vivo *Microscopy, Duke University Medical Center, Durham, North Carolina*

ABSTRACT

A precise knowledge of the myocardial fiber architecture is essential to accurately understand and interpret cardiac electrical and mechanical functions. Diffusion tensor imaging has been used to noninvasively and quantitatively characterize myocardial fiber orientations. However, because the approach necessitates diffusion to be measured in multiple encoding directions and frequently at multiple weighting levels, the required data set size may present a limitation on its acquisition time efficiency. Applying the principles of reduced encoding imaging (REI), four basic reconstruction schemes, keyhole using direct substitution, keyhole with baseline correction, symmetrically encoded REI with generalized-series reconstruction (RIGR), and asymmetrically encoded RIGR, are evaluated in terms of their accuracy in diffusion tensor fiber orientation mapping of excised myocardial samples. Results show that the performances of all REI schemes, at approximately 50% reduced encoding, are at least comparable with that of a control experiment consisting of proportionally reduced number of full k-space images. Moreover, although performances of the symmetrically and asymmetrically encoded RIGR schemes are similar, both methods provide significant improvements over the control experiment and the direct-substitution keyhole technique. These findings demonstrate the potential of the general REI methodology for diffusion tensor imaging and pave the way for modified schemes involving rapid imaging sequences or alternative k-space sampling strategies to achieve even better data acquisition time efficiency and performance.

Address correspondence and reprint requests to Edward W. Hsu.

Copyright © 2001 by Marcel Dekker, Inc. www.dekker.com

ORDER REPRINTS

Key Words: *Diffusion tensor imaging; Keyhole; Reduced encoding imaging; RIGR*

INTRODUCTION

The myocardial fiber architecture has been implicated in the pronounced anisotropy of electrical and mechanical behaviors in the heart. For example, electrical wavefront conduction velocity in the myocardium is reported to be two to three times faster along than across the orientations of myocardial fibers (1,2). Models of the myocardium based on generalized descriptions of structure have provided basic understanding of their functions. However, a precise quantitative knowledge of the tissue structure is needed to accurately account for functionally significant structural variations due to natural subject-to-subject heterogeneity or structural alterations associated with diseases, injury, or remodeling (3,4).

Compared with conventional histology, which normally requires destructive sectioning of the tissues examined, the noninvasive nature of magnetic resonance imaging makes it an attractive alternative for assessing tissue structure. By quantitatively characterizing the microstructure-induced anisotropy of water diffusion, MR diffusion tensor imaging (5) has been used to assess the fiber architecture of ordered tissues such as the brain white matter (6), spinal cord (7,8), cartilage (9), myocardium (10–12), and other musculature (13–15). One underlying hypothesis in these studies is that the eigenvector corresponding to the largest ranked diffusion tensor eigenvalue (i.e., the direction in which diffusion is fastest) coincides with the local tissue fiber orientation. In the myocardium, strong evidence to support the hypothesis has been found in the direct correlation of myocardial fiber orientations measured by magnetic resonance diffusion tensor imaging and conventional histologic techniques (16–18).

In three-dimensional space, the generalized diffusion tensor is a symmetric, second-order, 3×3 matrix. A unique solution to the six independent variables of the diffusion tensor requires diffusion to be quantified in at least six non-coplanar encoding gradient directions. A minimal diffusion tensor imaging experiment would thus consist of seven image acquisitions, including one nonweighted and one diffusion-weighted image in each of the six predetermined encoding directions. To increase the accuracy of the measurement, additional acquisitions, either by including more diffusion encoding directions, more encoding levels per direction, or a combination of both, are often used. The obvious drawback is that the additional acquisitions necessarily lengthen the required scan time and may therefore present a limitation on the time efficiency (i.e., temporal resolution) of these experiments. Because of the signal-to-noise ratio trade-off between scan time and image pixel size, the time efficiency limitation may alternatively represent a constraint in spatial resolution. Therefore, a means to achieve data acquisition time reduction without incurring the proportional loss in measurement accuracy is desirable to improve the time or spatial resolution of diffusion tensor imaging experiments.

Except for variations in the amplitudes of the diffusion encoding gradient pulses that specify the direction and magnitude of diffusion weighting, the typical diffusion tensor imaging resembles a dynamic imaging experiment in that the identical pulse sequence is repeated over time to encode image contrast changes. Because image contrast is primarily of low spatial frequency in nature, diffusion-weighted images may be reasonably reproduced from limited central k-space sampling via reduced encoding imaging (REI) techniques such as keyhole (19,20) and REI by generalized-series reconstruction (RIGR) (21,22). In general, these techniques require the acquisition of one or more full k-space ''reference'' data and a series of limited central k-space ''dynamic'' data. The dynamic data are then combined with the outer k-space of the reference data and reconstructed to produce images that are effectively obtained at higher temporal resolution but without the blurring and Gibbs artifacts normally associated with limited k-space sampling. Application of REI techniques to diffusion tensor imaging may, on the one hand, offer a direct means to improve the acquisition time efficiency of diffusion tensor imaging experiments based on conventional (e.g., spin echo) acquisitions. On the other hand, because REI involves primarily image reconstruction, the methodology may be combined with rapid imaging acquisitions to achieve even higher temporal resolution.

The goals of the current study are to investigate the applicability of the general REI approach and to evaluate the performances of specific REI reconstruction schemes for high-resolution fiber orientation mapping via diffusion tensor imaging in excised myocardial samples. The schemes examined are keyhole using direct k-space substitution, keyhole with a zeroth-order intensity and phase correction, symmetrically encoded RIGR, and asymmetrically encoded RIGR. Because the acquisition time effi-

Copyright © Marcel Dekker, Inc. All rights reserved.

ORDER REPRINTS

ciency gained via these REI approaches can be likewise achieved by simply decreasing the number of full k-space acquisitions in the diffusion tensor data set (i.e., using half of the full k-space images as opposed to using 50% reduced encoding in all images), performances of the REI schemes are evaluated against that of the latter ''control'' experiment.

MATERIALS AND METHODS

Full k-Space Diffusion Tensor Imaging

Diffusion tensor imaging data used in the present study are in part included in other studies described previously (16). Briefly, freshly excised canine heart right ventricle samples ($n = 6$) were imaged (4 multislice, 1.5-mm slice thickness, 30-mm filed of view, 128 readout points, and 64 phase encoding steps) in the short-axis plane using a 7.1-T Oxford instrument (Oxford, UK) with a modified spin echo sequence that minimized cross-terms between the diffusion encoding and imaging gradient pulses (14). For each experiment, diffusion of water was measured in six non-coplanar gradient directions given by $\mathbf{g}^T = (g_x, g_y, g_z) \in \{(1, 1, 0), (0, 1, 1), (1, 0, 1), (-1, 1, 0), (0, -1, 1), (1, 0, -1)\}$, with four pairs of equal, but opposite polarity, diffusion gradient amplitudes (eight levels total, absolute b values ranging from 1 to 360 sec/mm^2 per gradient axis) in each direction. Using the entire full k-space image data set (48 images in total), diffusion tensors were calculated and diagonalized off-line on a pixel-by-pixel basis via nonlinear least-squares curve-fitting according to the signal intensity attenuation equation

$$A(TE) = \exp\left(-(\mathbf{g}^T \cdot \mathbf{D} \cdot \mathbf{g})\gamma^2 \int_0^{TE} \left(\int_0^t G(\tau)d\tau\right)^2 dt\right) \quad (1)$$

The eigenvector corresponding to the largest ranked diffusion tensor eigenvalue, ev_1 (specifically $\mathbf{ev}_1^{full}$ for full k-space acquisitions), was taken to be the fiber orientation and was used as the ''gold standard'' for subsequent comparisons.

Reduced Encoding Diffusion Tensor Imaging

Diffusion-weighted images were reconstructed using data corresponding to the central 32 (either with or without asymmetric offset) of the original 64 full k-space phase encoding steps to simulate REI acquisitions. In principle, the diffusion tensor data set, which contains diffusion-weighted images encoded in multiple gradient directions and at multiple gradient amplitudes, allows several permutations in the choice of ''reference'' and ''dynamic'' images. For example, the image with the least diffusion weighting can be used as the reference in reconstructing other images encoded in the same gradient direction. Alternatively, images obtained in one gradient direction can be used as the reference for images encoded at the same gradient amplitude but in different directions. In practice, as is demonstrated in Fig. 1, data inconsistency (i.e., intensity and phase mismatch across the k-space boundaries of the reference and replacement data) presents a serious complication for REI reconstruction using direct data substitution across different diffusion-weighting levels. To alleviate the problem of data inconsistency, without loss of generality, the image acquired in the $g^T = (1, 1, 0)$ direction was arbitrarily chosen as

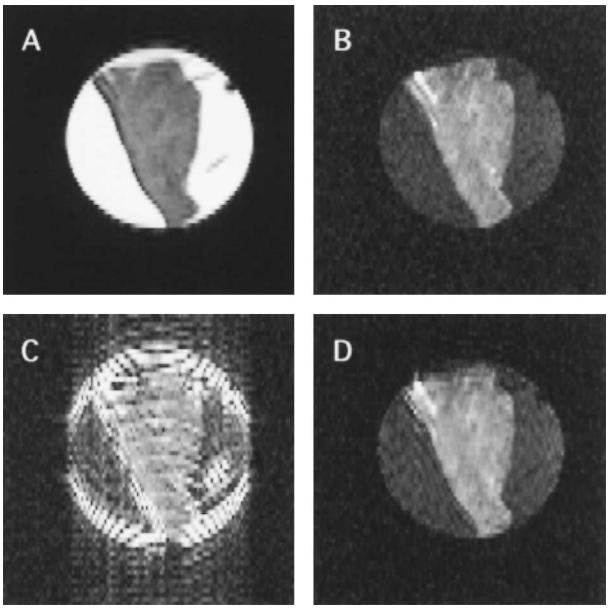

Figure 1. Effect of raw data inconsistency on reconstruction of reduced encoding diffusion-weighted images. For the short-axis view of the excised myocardial sample in a saline-filled tube, the least diffusion-weighted image (A) is used as the reference image in keyhole and RIGR reconstructions of the heavily weighted image (B). The direct-substitution keyhole image (C) suffers severe ringing and edge-enhancement artifacts due to intensity and phase discontinuities between the reference and replacement data. In contrast, the symmetrically encoded RIGR image (D) is relatively immune to this high-pass filtering effect. Images correspond to one slice of a four-multislice acquisition, and intensities as shown have been numerically scaled to match contrast in the myocardium.

Copyright © Marcel Dekker, Inc. All rights reserved.

ORDER REPRINTS

the reference in reconstructing images of the other five directions at each weighting level in the remainder of the present study.

For each sample, images were generated separately using each of four REI schemes, which are described below in the order of increasing complexity of the reconstruction algorithm:

1. Keyhole with direct data substitution (KD). Images were reconstructed using data taken symmetrically from the central 32 phase encoding steps (-15 to 16) of the full k-space data (consisting of steps -31 to 32). Following the original keyhole technique, the reduced encoding data were directly combined with the outer k-space reference data and Fourier transformed without correction.
2. Keyhole with zeroth-order correction (KC). This is the same as the approximate generalized-series (GS) reconstruction technique described previously (23). The scheme adds to the above keyhole method a zeroth order, or baseline, correction to match the signal intensity and phase differences between replacement and reference data. In this, the reference data are multiplied with a complex scalar correction factor, c_0, given by

$$c_0 = \frac{\sum\sum d^*_{ref}(k_x,k_y)d_{repl}(k_x,k_y)}{\sum\sum d^*_{ref}(k_x,k_y)d_{ref}(k_x,k_y)} \quad (2)$$

   calculated from the reference (d_{ref}) and replacement (d_{repl}) data over the central k-space region denoted by the variables k_x and k_y.
3. Symmetrically encoded RIGR (sRIGR). In contrast to the first two techniques, which are based on Fourier series representation, RIGR models image data parametrically as generalized-series functions. Information extracted from the dynamic data is then used to ''modulate'' the outer k-space reference data to perform higher orders of correction, hence achieving improved consistency between the dynamic and reference data. Details of the RIGR algorithm are beyond the scope of the present paper but can be found readily in the literature (21,23).
4. Asymmetrically encoded RIGR (aRIGR). In contrast to the above schemes that use symmetrically reduced phase encoding steps (i.e., steps -15 to 16), this scheme uses data extracted asymmetrically (i.e., using steps -7 to 24) of the full k-space data. Taking advantage of the complex conjugate property of the k-space data, the additional higher frequency phase encoding steps included by the asymmetric offset may provide higher accuracy in the reconstructed reduced encoding data.

Subsequent to generating the REI reconstructions, the diffusion-weighted images obtained for each REI scheme and the corresponding reference images were used to calculate diffusion tensors and fiber orientations as mentioned previously.

Control Experiment

All REI schemes described above are based on images reconstructed using 32 of the original 64 phase encoding steps (i.e., to achieve 50% acquisition time savings factor). As the basis for evaluating their performances, a control experiment was obtained by including half of the full k-space diffusion-weighted images (i.e., 24 of the original 48 images), comprised of the 4 images with the lowest and highest b values in each of the six diffusion encoding directions. As such, each reduced encoding diffusion tensor and the control experiment would have required approximately the same data acquisition time.

Statistical Analysis

Computed fiber orientations for each REI scheme (including the control experiment), denoted by $\mathbf{ev}_1^{red}$, are compared with the gold standard $\mathbf{ev}_1^{full}$ by determining their deviation angle $\Delta\alpha$ via their vector inner product according to

$$\Delta\alpha = \arccos(|\mathbf{ev}_1^{full} \cdot \mathbf{ev}_1^{red}|) \quad (3)$$

The deviation angles were averaged over the entire area of the sample. Single-factor, repeated-measures, analysis of variance (ANOVA) statistics (24) were performed to determine whether the deviation angles of the REI schemes and the control experiment (five groups total) are significantly different. Subsequently, applying the Bonferroni t tests to the 10 possible pair-wise post-hoc comparisons among the five groups, differences of group mean with $p < 0.005$ (i.e., $0.05/10 = 0.005$) were considered to be significant.

RESULTS

Figure 2 shows a four-multislice diffusion-weighted image and the gold standard fiber orientation map (i.e., obtained using the entire full k-space data set) of a representative myocardial sample. The fiber angle map demonstrates the classic epi-to-endocardial counterclockwise

Copyright © Marcel Dekker, Inc. All rights reserved.

ORDER REPRINTS

rotation of myocardial fibers. Deviation angle maps and their corresponding histograms obtained for each REI scheme and the control experiment for the same sample are shown in Fig. 3. In reference to the diffusion-weighted image (Fig. 2), the deviation angle map (Fig. 3) reveals generally small angular deviations. However, there are scattered points of larger errors mostly located at borders of the sample and in localized regions that have large signal intensity variations in the diffusion-weighted images.

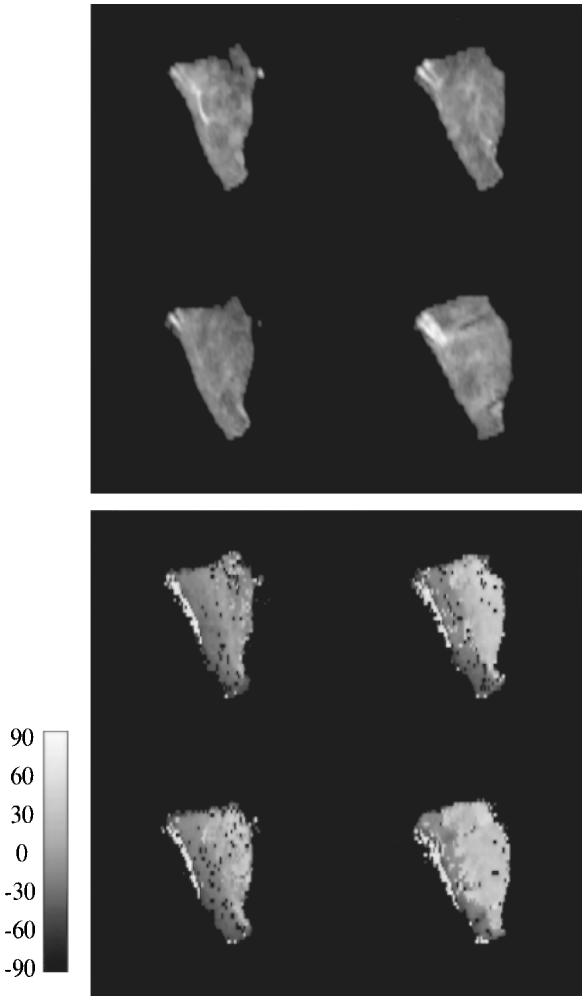

Figure 2. Magnetic resonance multislice image and corresponding fiber orientation map of a representative myocardial sample. The orientation map (right) represents the gold standard fiber inclination angles (in degrees, encoded in gray scale) with respect to the imaging plane and shows the fiber angles to undergo a counterclockwise rotation from the epicardium to the endocardium (left to right edge of the sample). Isolated pixels within the myocardium are missing due to failed diffusion tensor estimation or diagonalization. The data correspond to sample 4 in Table 1.

Individual sample-averaged deviation angles are tabulated in Table 1. The group means of deviation angles with respect to the gold standard for KD, KC, sRIGR, aRIGR, and the control experiment are 14.82 ± 1.99, 12.60 ± 1.50, 9.64 ± 1.12, 9.49 ± 1.27, and 14.73 ± 1.89 degrees (mean ± SEM, $n = 6$), respectively. Qualitatively, all REI schemes have deviation angles that are comparable or less than the control experiment, and there is a trend of decreasing deviation angle as the level of complexity of the REI reconstruction scheme increases. The ANOVA results in Table 2 reveal an F-test value of 12.73 ($p < 0.00003$), suggesting that at least one of the five groups examined is significantly different from the remaining groups. Subsequent post-hoc multiple comparison tests indicate that 4 of 10 pair-wise comparisons have significantly different group means: sRIGR versus control, aRIGR versus control, KD versus sRIGR, and KD versus aRIGR.

DISCUSSION

Results shown in Figs. 2 and 3 indicate that all REI schemes yielded fiber orientation maps that generally agree with the gold standard. Particularly, the mean deviation angles for the RIGR schemes (9.64 ± 1.12 degrees for sRIGR and 9.49 ± 1.27 degrees for aRIGR) are comparable with the 8.5-degree random error estimated from the 6-degree orientation measurement accuracy ($\sqrt{2} \times 6$ degrees = 8.5 degrees) previously reported for similar experiments (16). Because the REI approach is limited in encoding high spatial frequency (i.e., outer k-space) information, as expected there are points of larger deviation angles at borders of the sample and in isolated regions where image signal intensity variations are relatively large. Consequently, these isolated points are likely to have artificially inflated the mean deviation angles reported in Table 1, which are noticeably larger than the corresponding histogram peaks.

The ANOVA reveals that the performances of all REI schemes examined are at least comparable with the control. There is a trend that the performance is directly related to the level of complexity of the REI algorithm. Because the input data were identical, the varying performances are likely due to differences in reconstruction accuracy afforded by difference REI schemes. Specifically, the two RIGR-based schemes produced significantly lower deviation angles than both the KD scheme and the control experiment. However, asymmetric sampling ap-

Copyright © Marcel Dekker, Inc. All rights reserved.

ORDER REPRINTS

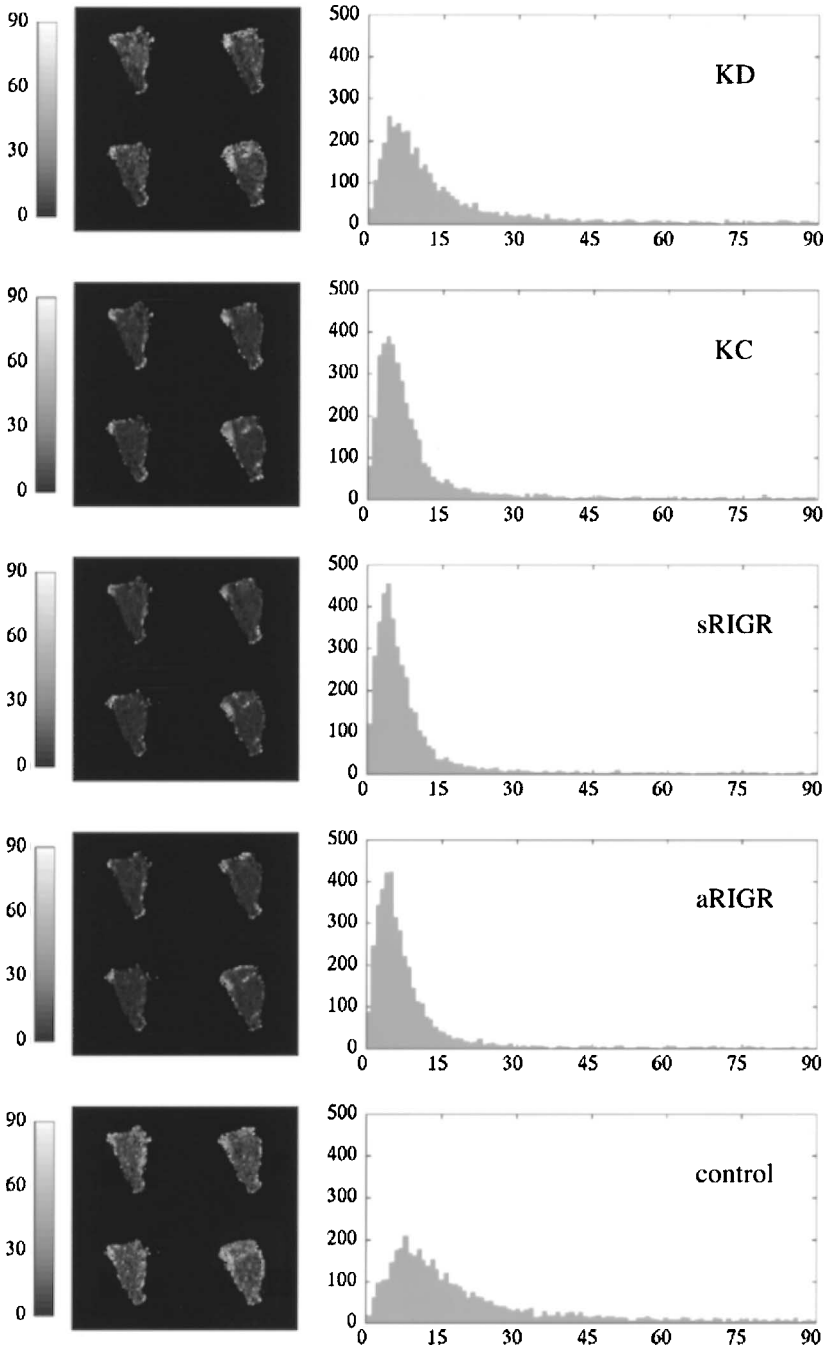

Figure 3. Deviation angle maps and histograms of myocardial fiber orientations obtained by reduced encoding and the control experiments. Deviation angles (in degrees) are shown in gray scale-coded maps (left). Data shown correspond to sample 4 in Table 1. The notations KD, KC, sRIGR, and aRIGR represent keyhole using direct data-substitution, keyhole with baseline correction, symmetrically encoded RIGR, and asymmetrically encoded RIGR, respectively.

Copyright © Marcel Dekker, Inc. All rights reserved.

ORDER REPRINTS

Table 1

Deviation Angles of Myocardial Fiber Orientations Obtained by REI and the Control with Respect to the Full k-Space Diffusion Tensor Imaging Experiment

Sample	KD	KC	sRIGR	aRIGR	Control
1	12.87	13.38	8.46	8.72	10.91
2	10.06	10.29	9.02	7.49	13.46
3	10.51	9.25	6.69	6.18	8.53
4	14.92	9.70	8.32	8.57	18.87
5	17.68	14.06	10.87	11.11	16.03
6	22.89	18.88	14.51	14.89	20.55
Mean	14.82	12.60	9.64	9.49	14.73
SEM	1.99	1.50	1.12	1.27	1.89

Each entry represents the mean over the area of the sample. Values are degrees. KD, keyhole with direct data substitution; KC, keyhole with zeroth-order correction; sRIGR, symmetrically encoded RIGR; aRIGR, asymmetrically encoded RIGR.

pears not to offer additional improvement compared with symmetrically sampled RIGR, suggesting that the two RIGR-based schemes may have reached the limit where the performance (i.e., average fiber orientation deviation angle from the gold standard) is dominated by random errors of subtraction. Combined, these results indicate that at least for myocardial fiber orientation mapping at 50% reduced encoding, the RIGR approach can be used to improve the efficiency of diffusion tensor studies, with less than the proportional loss in accuracy associated with acquisition time reduction.

Table 2

Single-Factor Repeated-Measures ANOVA and Post-Hoc Multiple Comparison Results of Myocardial Fiber Orientation Deviation Data in Table 1

ANOVA		
Five repeated measurements (n= 6)	F statistics 12.73	p 0.00003*
Post-hoc Paired Comparison	**Student t Value**	**p**
KD-control	0.087	0.93
KC-control	−2.06	0.052
sRIGR-control	−4.92	0.00008*
aRIGR-control	−5.06	0.00006*
KD-KC	2.15	0.044
KD-sRIGR	5.00	0.00007*
KC-sRIGR	2.85	0.0098
KD-aRIGR	5.15	0.00005*
KC-aRIGR	3.00	0.0071
sRIGR-aRIGR	0.146	0.89

KD, keyhole with direct data substitution; KC, keyhole with zeroth-order correction; sRIGR, symmetrically encoded RIGR; aRIGR, asymmetrically encoded RIGR.

*Significant F or Student t statistics, corresponding to $p < 0.05$ and $p < 0.005$ (Bonferroni condition for 10 multiple comparisons with an overall $p < 0.05$), respectively.

Although significant efficiency improvements require the use of RIGR or similar reconstruction-intensive REI algorithms, the simpler techniques (e.g., KD and KC) may also be advantageous for diffusion tensor imaging, especially in situations where the number of image acquisitions is already at the minimum. It is known that the accuracy of diffusion tensor imaging experiments is dependent on the choice of diffusion encoding directions (25,26) and that using, for example, an optimized set of 12 encoding directions (25) is generally better than doubling the acquisitions based on any six-direction combinations. Because the performances of all REI schemes are at least comparable with that of an experiment involving proportionally decreased acquisitions (i.e., the control), the combination of the optimized 12-direction scheme and 50% REI, with or without any data consistency correction, would thus offer a better trade-off between acquisition time efficiency and accuracy than using a six-direction scheme with full k-space acquisitions.

In summary, REI was applied to myocardial fiber orientation mapping using diffusion tensor imaging, and performances of four basic REI schemes were evaluated and compared with a control experiment consisting of proportionally decreased full k-space images. Results indicate that the performances of all REI schemes examined are at least comparable with that of the control experiment. Importantly, RIGR, with either symmetric or asymmetric sampling, leads to significantly improved

Copyright © Marcel Dekker, Inc. All rights reserved.

ORDER REPRINTS

performance over both the control and direct substitution keyhole method. Although the REI schemes examined correspond to an acquisition time reduction of 42% (for every six images were generated from one full and five one-half acquisitions), the present study does not preclude alternative REI schemes for achieving even better efficiency and performance. Possible variations to consider include (a) increasing the factor of reduced encoding by reconstructing from fewer phase encoding steps, (b) combining REI with rapid imaging techniques such as fast spin echo (27,28) and echo planar (29) acquisitions, (c) using alternative k-space sampling trajectories such as radial (30) or spiral (31,32) sampling that inherently oversamples the central k-space, and (d) if hardware permits, coupling REI with the use of receiver coil arrays and parallel acquisition schemes such as SMASH (simultaneous acquisition of spatial harmonics) (33) and SENSE (sensitivity encoding) (34). To this end, findings of the present study may serve a useful starting point for these future investigations.

ACKNOWLEDGMENTS

We gratefully acknowledge the technical support in RIGR reconstruction from Drs. Z. P. Liang and C. Hess and the editorial assistance of Mrs. E. Fitzsimons. Supported in part by National Institutes of Health National Center for Research Resources (grant P41RR05959) and the American Heart Association (grant B98425N).

REFERENCES

1. Roberts, D.E.; Lawrence, T.H.; Scher, A.M. Influence of Cardiac Fiber Orientation on Wavefront Voltage, Conduction Velocity, and Tissue Resistivity in the Dog. Circ. Res. **1979**, *44*, 701–712.
2. Clerc, L. Directional Differences of Impulse Spread in Trabecular Muscle From Mammalian Heart. J. Physiol. **1975**, *255*, 335–346.
3. Ursell, P.C.; Gardner, P.I.; Albala, A.; Fenoglio, Jr. J.J.; Wit, A.L. Structural and Electrophysiological Changes in the Epicardial Border Zone of Myocardial Infarcts During Infarct Healing. Circ. Res. **1985**, *56*, 436–452.
4. Wickline, S.A.; Verdonk, E.D.; Wong, A.K.; Shepard, R.K.; Miller, J.G. Structural Remodeling of Human Myocardial Tissue After Infarction. Quantification With Ultrasonic Backscatter. Circulation **1992**, *85*, 259–268.
5. Basser, P.J.; Mattiello, J.; LeBihan, D. MR Diffusion Tensor Spectroscopy and Imaging. Biophys. J. **1994**, *66*, 259–267.
6. Pierpaoli, C.; Jezzard, P.; Basser, P.J.; Barnett, A.; Di Chiro, G. Diffusion Tensor MR Imaging of the Human Brain. Radiology **1996**, *201*, 637–648.
7. Inglis, B.A.; Yang, L.; Wirth, E.D.; Plant, D.; Mareci, T.H. Diffusion Anisotropy in Excised Normal Rat Spinal Cord Measured by NMR Microscopy. Magn. Reson. Imaging **1997**, *15*, 441–450.
8. Gulani, V.; Iwamoto, G.A.; Jiang, H.; Shimony, J.S.; Webb, A.G.; Lauterbur, P.C. A Multiple Echo Pulse Sequence for Diffusion Tensor Imaging and Its Application in Excised Rat Spinal Cords. Magn. Reson. Med. **1997**, *38*, 868–873.
9. Hsu, E.W.; Setton, L.A. Diffusion Tensor Microscopy of the Intervertebral Disc Anulus Fibrosus. Magn. Reson. Med. **1999**, *41*, 992–999.
10. Garrido, L.; Wedeen, V.J.; Kwong, K.K.; Spencer, U.M.; Kantor, H.L. Anisotropy of Water Diffusion in the Myocardium of the Rat. Circ. Res. **1994**, *74*, 789–793.
11. Reese, T.G.; Weisskoff, R.M.; Smith, R.N.; Rosen, B.R.; Dinsmore, R.E.; Wedeen, V.J. Imaging Myocardial Fiber Architecture In Vivo With Magnetic Resonance. Magn. Reson. Med. **1995**, *34*, 786–791.
12. Tseng, W.I.; Reese, T.G.; Weisskoff, R.M.; Brady, T.J.; Wedeen, V.J. Myocardial Fiber Shortening in Humans: Initial Results of MR Imaging. Radiology **2000**, *216*, 128–139.
13. Basser, P.J.; Mattiello, J.; LeBihan, D. Estimation of the Effective Self-Diffusion Tensor from the NMR Spin Echo. J. Magn. Reson. Ser. B **1994**, *103*, 247–254.
14. Hsu, E.; Mori, S. Analytical Expressions for the NMR Apparent Diffusion Coefficients in an Anisotropic System and a Simplified Method for Determining Fiber Orientation. Magn. Reson. Med. **1995**, *34*, 194–200.
15. van Doorn, A.; Bovendeerd, P.H.M.; Nicolay, K.; Drost, M.R.; Janssen, J.D. Determination of Muscle Fibre Orientation Using Diffusion-Weighted MRI. Eur. J. Morphol. **1996**, *34*, 5–10.
16. Hsu, E.W.; Muzikant, A.L.; Matulevicius, S.A.; Penland, R.C.; Henriquez, C.S. Magnetic Resonance Myocardial Fiber-Orientation Mapping With Direct Histological Correlation. Am. J. Physiol. **1998**, *274*, H1627–H1634.
17. Scollan, D.F.; Holmes, A.; Winslow, R.; Forder, J.R. Histological Validation of Myocardial Microstructure Obtained From Diffusion Tensor Magnetic Resonance Imaging. Am. J. Physiol. **1998**, *275*, H2308–H2318.
18. Holmes, A.A.; Scollan, D.F.; Winslow, R.L. Direct Histological Validation of Diffusion Tensor MRI in Formaldehyde-Fixed Myocardium. Magn. Reson. Med. **2000**, *44*, 157–161.
19. van Vaals, J.J.; Brummer, M.E.; Dixon, W.T.; Tuithof, H.H.; Engels, H.; Nelson, R.C.; Gerety, B.M.; Chezmar, J.L.; den Boer, J.A. ''Keyhole'' Method for Accelerating Imaging of Contrast Agent Uptake. JMRI **1993**, *3*, 671–675.
20. Jones, R.A.; Haraldseth, O.; Müller, T.B.; Rinck, P.A.; Øksendal, A.N. k-Space Substitution: A Novel Dynamic

Copyright © Marcel Dekker, Inc. All rights reserved.

ORDER REPRINTS

Imaging Technique. Magn. Reson. Med. **1993,** *29*, 830–834.
21. Liang, Z.P.; Boada, F.; Constable, T.; Haacke, E.M.; Lauterbur, P.C. Constrained Reconstruction Methods in MR Imaging. Rev. Magn. Reson. Med. **1992**, *4*, 67–185.
22. Webb, A.G.; Liang, Z.P.; Magin, R.L.; Lauterbur, P.C. Applications of Reduced-Encoding MR Imaging With Generalized-Series Reconstruction (RIGR). JMRI **1993**, *3*, 925–928.
23. Liang Z.P.; Lauterbur, P.C. An Efficient Method for Dynamic Magnetic Resonance Imaging. IEEE Trans. Med. Imaging **1994**, *13*, 677–686.
24. Glantz, S.A. *Primer of Biostatistics*; McGraw-Hill: New York, 1997.
25. Papadakis, N.G.; Xing, D.; Huang, C.L.; Hall, L.D.; Carpenter, T.A. A Comparative Study of Acquisition Schemes for Diffusion Tensor Imaging Using MRI. Magn. Reson. Imaging **1999**, *17*, 881–892.
26. Jones, D.K.; Horsfield, M.A.; Simmons, A. Optimal Strategies for Measuring Diffusion in Anisotropic Systems by Magnetic Resonance Imaging. Magn. Reson. Med. **1999**, *42*, 515–525.
27. Hennig, J.; Naureth, A.; Friedburg, H. RARE Imaging: A Fast Imaging Method for Clinical MR. Magn. Reson. Med. **1986**, *3*, 823–833.
28. Mulkern, R.V.; Wong, S.T.S.; Winalski, C.; Jolesz, F.A. Contrast Manipulation and Artifact Assessment of 2D and 3D RARE Sequences. Magn. Reson. Imaging **1990**, *8*, 557–566.
29. Mansfield, P. Multiplanar Image Formation Using NMR Spin Echoes. J. Phys. C **1977**, *10*, L55–L58.
30. Glover, G.; Pauly, J. Projection Reconstruction Techniques for Reduction of Motion Effects in MRI. Magn. Reson. Med. **1992**, *28*, 275–289.
31. Blum, M.J.; Braun, M.; Rosenfeld, D. Fast Magnetic Resonance Imaging Using Spiral Trajectories. Austr. Phys. Eng. Sci. Med. **1987**, *10*, 79–87.
32. Meyer, C.H.; Hu, B.S.; Nishimura, D.G.; Macovski, A. Fast Spiral Coronary Artery Imaging. Magn. Reson. Med. **1992**, *28*, 202–213.
33. Sodickson, D.K.; Manning, W.J. Simultaneous Acquisition of Spatial Harmonics (SMASH): Fast Imaging with Radiofrequency Coil Arrays. Magn. Reson. Med. **1997**, *38*, 591–603.
34. Pruessmann, K.P.; Weiger, M.; Scheidegger, M.B.; Boesiger, P. SENSE: Sensitivity Encoding for Fast MRI. Magn. Reson. Med. **1999**, *42*, 952–962.

Received September 27, 2000
Accepted May 10, 2001

Copyright © Marcel Dekker, Inc. All rights reserved.

Request Permission or Order Reprints Instantly!

Interested in copying and sharing this article? In most cases, U.S. Copyright Law requires that you get permission from the article's rightsholder before using copyrighted content.

All information and materials found in this article, including but not limited to text, trademarks, patents, logos, graphics and images (the "Materials"), are the copyrighted works and other forms of intellectual property of Marcel Dekker, Inc., or its licensors. All rights not expressly granted are reserved.

Get permission to lawfully reproduce and distribute the Materials or order reprints quickly and painlessly. Simply click on the "Request Permission/Reprints Here" link below and follow the instructions. Visit the U.S. Copyright Office for information on Fair Use limitations of U.S. copyright law. Please refer to The Association of American Publishers' (AAP) website for guidelines on Fair Use in the Classroom.

The Materials are for your personal use only and cannot be reformatted, reposted, resold or distributed by electronic means or otherwise without permission from Marcel Dekker, Inc. Marcel Dekker, Inc. grants you the limited right to display the Materials only on your personal computer or personal wireless device, and to copy and download single copies of such Materials provided that any copyright, trademark or other notice appearing on such Materials is also retained by, displayed, copied or downloaded as part of the Materials and is not removed or obscured, and provided you do not edit, modify, alter or enhance the Materials. Please refer to our Website User Agreement for more details.

Order now!

Reprints of this article can also be ordered at
http://www.dekker.com/servlet/product/DOI/101081JCMR100108588